Tungsten (2024) 6:585–595
https://doi.org/10.1007/s42864-023-00253-x

Tungsten
www.springer.com/42864

ORIGINAL PAPER

Dual template-induced construction of three-dimensional porous SiO_2/NC/Co-CNTs heterostructure with highly dispersed active sites for efficient oxygen evolution reaction

Hai-Qi Zhang[1] · Xiao-Jun Zeng[1] · Qing-Qing Zhang[1] · Zu-Liang Zhang[1] · Chu-Long Jin[1] · Rong-Hai Yu[2]

Received: 22 July 2023 / Revised: 9 September 2023 / Accepted: 11 September 2023 / Published online: 6 December 2023

Abstract
The development and exploration of efficient and economical electrocatalysts for oxygen evolution reaction (OER) represents the main bottleneck to unlocking a sustainable energy scenario based on electrocatalytic water splitting. Nanoscale integration of three-dimensional (3D) porous heterostructure with highly dispersed active sites and good structural stability is challenging. Herein, a dual template route is developed to construct the 3D porous SiO_2/nitrogen-doped carbon (NC)/Co-carbon nanotubes (CNTs) heterostructure. Importantly, the hard template (SiO_2 nanospheres) contributes to 3D porous structure, increases the specific surface area, and promotes the contact area of the electrolyte. At the same time, the soft template (basic zinc carbonate) can control the growth of 1D CNTs and facilitate the exposure of the active sites. Apparently, 3D porous SiO_2/NC/Co-CNTs heterostructure inherits highly dispersed Co nanoparticles coated by NC. CNTs conductive channels and abundant N heteroatoms doping are reasonably constructed by a dual template strategy. Therefore, SiO_2/NC/Co-CNTs catalyst provides an extraordinary activity for the OER in alkaline media, with a low overpotential of 298 mV at a current density of 10 mA·cm^{-2}. Furthermore, SiO_2/NC/Co-CNTs heterostructure enables excellent long-term durability with a 10 mV decay in overpotential after 3000 cyclic voltammetry cycles, and 97% remain in current density over 20 h. It is believed that this dual template strategy can provide a new and simple way to construct a highly dispersed active site in electrocatalysts.

Keywords Dual template · High dispersion · Porous heterostructure · Conductive channels · Oxygen evolution reaction

1 Introduction

The continued use of fossil fuels (oil, coal, natural gas, etc.) leads to energy shortages and climate extremes that are becoming increasingly serious [1, 2]. Therefore, people are constantly exploring cheap, clean, and renewable energy [3]. Notably, due to its superior energy density, source environmental protection, and zero carbon footprint, hydrogen has been considered to be the most promising renewable energy source at present [4, 5]. In many hydrogen production, electrochemical water decomposition hydrogen production is an efficient way to meet energy needs and solve environmental pollution [6]. For water electrolysis, the anodic oxygen evolution reaction (OER) ($4OH^-(aq) \rightarrow O_2(g) + 2H_2O(l) + 4e^-$) is the main obstacle to hydrogen production because OER is a rather complex four-electron reaction process, including O–H bond cleavage, O–O bond formation, and proton-coupled electron transfer steps [7, 8]. Thus, it is necessary for OER electrocatalysts to have a small overpotential to accelerate the reaction kinetics. So far, precious metal-based catalysts (e.g., IrO_2 and RuO_2) are still widely used in OER electrocatalysts [9, 10]. However, their low earth reserves and high price limit their widespread application. In this context, it is necessary to develop cost-effective and highly reactive non-precious metal OER electrocatalysts derived from earth-abundant elements [11, 12].

Among the numerous transition metal alternatives, cobalt is considered a promising non-noble metal OER

Hai-Qi Zhang and Xiao-Jun Zeng contributed equally to this work.

✉ Xiao-Jun Zeng
zengxiaojun@jcu.edu.cn

[1] School of Materials Science and Engineering, Jingdezhen Ceramic University, Jingdezhen 333403, China

[2] School of Materials Science and Engineering, Beihang University, Beijing 100191, China

electrocatalyst [13]. Especially, it is believed that the highly dispersed Co nanocatalysts can be used as efficient OER catalysts due to the exposed active sites [14]. So far, several methods have been developed to obtain highly dispersed Co nanoparticles, and the typical synthesis strategies are mainly solid-state diffusion strategies and pyrolysis strategies. The solid-state diffusion strategy includes the top-down strategy. The pyrolysis method, combined with wet chemical methods, is a typical cost-effective route that can easily fix a single atomic site onto a carbon substrate, achieving both porous structure and highly dispersed metal single points [15–18]. However, currently cobalt-based nanocatalysts face challenges as they exhibit relatively poor electrical conductivity and uncontrollable aggregation during long-term operation, resulting in insufficient exposure of active components and insufficient long-term electrolytic stability. The strategies to address these issues include physical confinement (e.g., soft or hard template), heteroatom doping (e.g., N, P, and S), and *in situ* induced high conductivity support.

Carbon, such as graphene and graphitic carbon, is an ideal carrier material for monodisperse nanocatalysts due to its high specific surface area and good electrical conductivity [19]. The carbon derived from urea/glucose combined with a soft template can provide a highly porous structure with abundant nitrogen heteroatoms doping, which generates favorable electron migration channels and enhances the conductivity of the catalyst [20]. For example, Wang and co-workers prepared a highly dispersed Co atom-anchored N-doped porous carbon (p–Co–N–C) catalyst by a pyrolytic-alkali-acidizing tactic, which showed excellent electrosynthesis performance of H_2O_2 in an acidic environment [21]. On the other hand, the hard template route for producing functional carbon matrix using inorganic materials such as SiO_2, Santa Barbara Amorphous-15 (SBA-15), and NaCl is a promising option for the construction of porous heterostructures. This process involves finely controlled nano-casting processes to replicate the shape and structure of hard templates and build ordered pore materials. Due to the advantages of inexpensive and poisonless, it has been widely used to construct three-dimensional (3D) porous heterostructures with high conductivity and stable structures. For instance, Lou and co-workers prepared SiO_2 nanospheres as hard templates [22]. Subsequently, the nitrogen-doped hollow carbon spheres interconnected 3D fiber network with tin nanoparticles were successfully prepared by hydrolysis, electrospinning, annealing, and etching. Furthermore, Liu et al. reported *in situ* Fe monoatomically dispersed N,S co-doped (FeSA/NSC) stratified ordered porous carbon framework through one-step pyrolysis of dopamine/Fe^{3+} complexes and thiourea in the SBA-15 channel, which exhibited more outstanding electrocatalytic performance than Pt/C catalysts [23]. Although some achievements have been made in developing high-performance catalysts using a single template, there are still some problems that need to be improved in single template-derived heterostructures, such as unsatisfactory structural configuration and pore distribution, difficulty in completely removing hard templates, and few 2D units in 3D heterostructures. In contrast, dual template, which can generate higher specific surface area and expose more active sites, has emerged as an effective strategy to enhance electrocatalytic activity [24, 25]. For example, Zhong et al. developed a Co/CoO_x nano-heterojunctions encapsulated into nitrogen-doped carbon sheets (NCS@Co/CoO_x) via a dual-template-guided approach [24]. The prepared NCS@Co/CoO_x exhibited good OER activity with an overpotential of 350 mV at a current density of 10 mA·cm^{-2}.

To this end, a dual template strategy combing hard and soft templates has been proposed. The dual template not only combines the advantages of the hard template, that is, to promote the exposure of the active site and the contact area of the electrolyte through the limiting effect, but also combines the advantages of the soft templates, that is, to enhance the conductivity of the material and promote the formation of the highly dispersed active site. This provides a highly dispersed active site and an ideal carrier with high conductivity for the rational design of the catalyst, and alleviates the oxidation of the active site in the OER process. Therefore, in this study, SiO_2 nanospheres are used as hard templates, basic zinc carbonate is used as soft templates, and highly dispersed metal Co nanoparticles are wrapped in N-doped graphitized carbon (NC) and carbon nanotubes (CNTs) by simple physical grinding mixing and high-temperature pyrolysis strategies to form 3D porous heterostructures with high electrical conductivity and structural stability. The 3D porous structure, high specific surface area, highly dispersed Co nanoparticles, CNTs conductive channels, and abundant nitrogen heteroatoms doping promote the constructed SiO_2/NC/Co-CNTs catalyst to provide robust electrocatalytic OER activity and excellent stability in the alkaline electrolyte.

2 Experimental

2.1 Synthesis of SiO_2 nanospheres

Uniform SiO_2 nanospheres were prepared by Stöber method [26, 27]. Typically, 8 mmol of tetraethyl orthosilicate (TEOS, 93.2 wt.% ~ 93.6 wt.%) was dissolved in 16 mL of H_2O and 92 mL of ethanol. After stirring for 30 min, 3 mL of concentrated ammonia hydroxide (NH_4OH, 25 wt.% ~ 28 wt.%) was added quickly and continued stirring for 2 h. The resulting mixed solution was collected by centrifugation at high speed and washed several times with deionized water and ethanol (C_2H_6O, ≥ 95 wt.%). Finally, the powder was placed in a drying oven at 70 °C for 12 h.

2.2 Synthesis of SiO_2/NC/Co-CNTs catalysts

0.6 mmol of cobalt nitrate hexahydrate ($Co(NO_3)_2{\cdot}6H_2O$, ≥ 98.5 wt.%), 2.8 mmol of glucose (52.5 wt.% ~ 53 wt.%), and 40 mmol of urea (≥ 99 wt.%) were dispersed in 20 mL of deionized water. After awaiting for 15 min, 0.5 g of SiO_2 was added and continued stirring for 15 min, then ultrasonicated for 15 min. The resulting mixture was dried overnight in a vacuum at 80 °C. 0.3 g of the obtained powder and 0.3 g of basic zinc carbonate (Zn ≥ 57.0 wt.%) were added to a mortar and ground for 30 min. The ground samples were placed in a porcelain boat and heat-treated in an Ar atmosphere in a tube furnace. The samples were first kept at 550 °C for 2 h, and then kept at 1000 °C for 1 h and waited for natural cooling, with a heating rate of 5 °C·min^{-1}. For comparison, the additional amount of urea (400 mmol, 4 mmol) was optimized to achieve a higher electrocatalytic activity.

2.3 Synthesis of SiO_2/NC/Co and NC/Co-CNTs catalysts

To investigate the role of basic zinc carbonate in the construction of a soft template, a contrast catalyst without basic zinc carbonate, marked as SiO_2/NC/Co, was prepared with other parameters unchanged. Furthermore, the additional amount of basic zinc carbonate (0.15 g, 0.45 g) was optimized. At the same time, to further explore the impact of the SiO_2 hard template on electrocatalytic performance, catalysts with different SiO_2 addition amounts (0, 0.3, 0.6 g) were prepared. The catalyst without adding SiO_2 was labeled as NC/Co-CNTs.

2.4 Alkaline etching of SiO_2/NC/Co-CNTs (AE-SiO_2/NC/Co-CNTs) catalysts

To understand the role of the hard template, the SiO_2 hard template in SiO_2/NC/Co-CNTs catalysts was alkaline-etched. In a word, the SiO_2/NC/Co-CNTs catalysts were dissolve in 2 mol·L^{-1} NaOH aqueous solution (100 mL) and kept at 50 °C for 8 h. The mixture was collected by centrifugation and washed several times with H_2O. The obtained product (AE-SiO_2/NC/Co-CNTs) was dried in a vacuum oven at 80 °C for 24 h.

2.5 Characterization

Field emission scanning electron microscope (FESEM, SU-8010, HITACHI, Japan) and energy-dispersive X-ray spectroscopy (EDS, Oxford, Xplore, England) were used to observe the morphology and elemental content of the catalyst. At the same time, transmission electron microscopy (TEM, JEM-2100F, JEOL, Japan) was used to investigate the internal microstructure of the catalyst. Furthermore, the phases of catalysts were determined by X-ray diffraction (XRD, D8-Advance, Bruker, Germany). Additionally, X-ray photoelectron spectroscopy (XPS, Thermo escalab 250Xi, America) was conducted to analyze the chemical composition and element valence state of the catalyst. Micromeritics surface area analyzer (BRT, ASAP2020 M, Micromeritics, America) was used to test the Brunauer–Emmett–Teller (BET) specific surface area and pore size distribution of the catalyst.

2.6 Electrochemical measurements

The classic three-electrode system was used to evaluate the performance of the catalysts. The platinum wire, saturated Ag/AgCl, and glass carbon (diameter of 3 mm) were selected as the counter, reference, and working electrodes, respectively. Furthermore, all electrochemistry performance tests were finished in KOH (1 mol·L^{-1}) electrolyte, and analyzed by an electrochemical workstation (CHI 760E, Shanghai Huachen Instrument Co., Ltd., China) equipped with a rotation apparatus (RRDE-3A, ALS Inc., Tokyo, Japan), and prepared the working electrode as follows: 4 mg catalyst was added into Nafion solution (5 wt.%, 1 mL), and after ultrasonic treatment for 2 h, the obtained catalyst ink was dropped on the working electrode with a load of 0.2 mg·cm^{-2}. The electrochemical properties of the catalysts were evaluated by cyclic voltammetry (CV), linear sweep voltammetry (LSV), and the electrochemical impedance spectrum (EIS). Double-layer capacitance (C_{dl}) is obtained by recording CV curves at different scanning rates (20, 40, 60, 80, and 100 mV·s^{-1}). LSV curves were operated at a scan rate of 5 mV·s^{-1}. The catalyst stability was evaluated at constant potential. The EIS measurements were tested in the frequency range from 0.01 Hz to 100 kHz at an alternating current voltage (AC) of 5 mV. The measured Ag/AgCl potential is converted into a reversible hydrogen electrode (RHE) by the formula $E_{(RHE)} = E_{(Ag/AgCl)} + 0.0591 \times pH + 0.197$ ($E_{(RHE)}$: reversible hydrogen potential, $E_{(Ag/AgCl)}$: reference electrode potential, pH: pH value of the electrolyte) [28].

3 Results and discussion

A schematic diagram of the straightforward fabrication process and the synthetic chemistry involved for SiO_2/NC/Co-CNTs is shown in Fig. 1. Specifically, hard template (silica nanospheres), carbon sources, nitrogen sources, and metal sources were mixed in an agate mortar. Then, the SiO_2/NC/Co-CNTs catalyst was obtained by simple physical grinding mixing and high-temperature pyrolysis of the dried drug and the soft template accelerant zinc carbonate ($Zn_2(OH)_2CO_3$) in an appropriate ratio. The highly dispersed metal Co

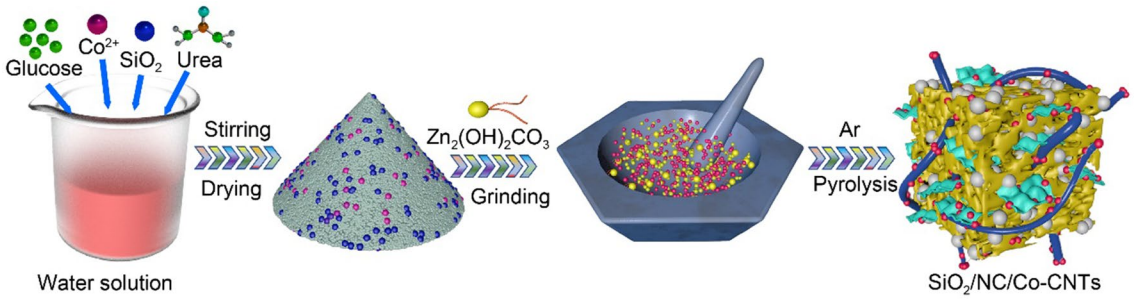

Fig. 1 Schematic illustration of the formation for SiO_2/NC/Co-CNTs

nanoparticles are mosaiced in NC, and promoted the formation of CNTs. The presence of NC in composites can prevent metal nanoparticles from being exposed to alkalis to cause dissolution or aggregation [29], thereby improving the stability of active species [30]. As a result, a 3D porous heterostructure with high conductivity and stable structure is constructed. Importantly, SiO_2 nanospheres, as a hard template, have a limiting effect. During the high-temperature pyrolysis, glucose-derived carbon is wrapped on the surface of SiO_2 nanospheres, which significantly increases the specific surface area and promotes the contact area of the electrolyte. Furthermore, silica nanospheres typically have rich pore structures that can be used as adsorption and storage areas for reactive substances. Meanwhile, the pore structure helps improve the accessibility of reactants, making it easier to reach the catalyst surface, thereby enhancing reaction kinetics. In addition, Co^{2+} will catalyze urea to form NC during pyrolysis, which can effectively improve the conductivity of the catalyst. At the same time, the graphitized carbon has the effect of carbothermal reduction [31]. It promotes the formation of highly dispersed metallic Co nanoparticles under the limited domain, which provides a highly dispersed active site and alleviates the oxidation of the active site during the OER process. Finally, basic zinc carbonate is used as a soft template accelerator to achieve the controlled growth of 1D CNTs [32]. The basic zinc carbonate can be decomposed at 1000 °C, leaving a porous structure and further facilitating the exposure of the active sites. For the catalyst obtained without the addition of basic zinc carbonate (SiO_2/NC/Co), no CNTs are found, as described below.

The crystal phases of the catalysts were investigated by XRD. As manifested in Fig. 2a, the peak at ~ 26.3° is the (002) face of graphitic carbon [33]. Three distinct strong peaks located at 44.2°, 51.5°, and 75.9° are attributed to the (111), (200), and (220) faces of metal Co (JCPDS No. 15-0806), respectively [34], confirming the formation of metallic Co. The broad peak at ~ 21° is attributed to SiO_2 (JCPDS No. 76-0939). By observing the XRD pattern of AE-SiO_2/NC/Co-CNTs, it is found that the peaks everywhere can be matched with the SiO_2 phase (JCPDS No. 77-1060), and the peak of Co basically disappears, which may be attributed to the strong crystallinity of SiO_2 at high temperature [35, 36]. XPS investigates each element's surface compositions and valence states in SiO_2/NC/Co and SiO_2/NC/Co-CNTs catalysts. The XPS survey spectra in Figs. S1, S2 identify the presence of Co, Si, N, O, and C elements, and the loading content of Co is around 0.8 at.%. The high-resolution of the Co 2p spectrum shows two main fitted peaks at 781.3 eV (Co $2p_{3/2}$) and 796.8 eV (Co $2p_{1/2}$), as well as two corresponding satellite peaks at 786.9 eV and 804.1 eV (Fig. 2b) [37]. The signal located in the Co $2p_{3/2}$ and Co $2p_{1/2}$ regions can be easily identified as Co–N bonds [38]. The high-resolution of the Si 2p spectrum is decomposed into four peaks at 102.4, 103.2, 103.8, and 104.4 eV (Fig. 2c), corresponding to Si_2O, SiO, Si_2O_3, and SiO_2 [39]. The high-resolution N 1 s spectrum is well decomposed into five peaks (Fig. 2d), namely pyridinic-N (402.8 eV), Co–N (399.9 eV), pyrrolic-N (399.1 eV), graphite-N (401.0 eV), and oxide-N (398.4 eV). Among them, the content of pyridinic-N and graphite-N, considered as efficient active components for the OER process [40], is the highest (Fig. S3). The presence of Co–N species through the coordination of surface Co with electronegative N elements further confirms the strong interaction between Co nanoparticles and N-doped carbon matrix [41]. The high-resolution C 1s spectrum has two main fitting peaks of 285.1 and 286.0 eV (Fig. 2e), which can be ascribed to C–C and C–N, respectively. The other two peaks centered at 284.5 and 288.3 eV are attributed to C = C and O = C, respectively [42, 43]. The presence of C–N bonds indicates the successful coupling of N heteroatoms into the carbon matrix. Because N heterogeneous atoms are very electronegative, N doping can alter the electron cloud distribution of adjacent C atoms, thereby enhancing the intermediate product adsorption capacity of catalysts [44]. In addition, two peaks can be separated in the high-resolution O 1s spectrum (Fig. 2f). The peaks observed at 533.1 and 530.8 eV can be attributed to surface absorbed O and C–O, respectively, which is due to slight oxidation of the metal [45–47].

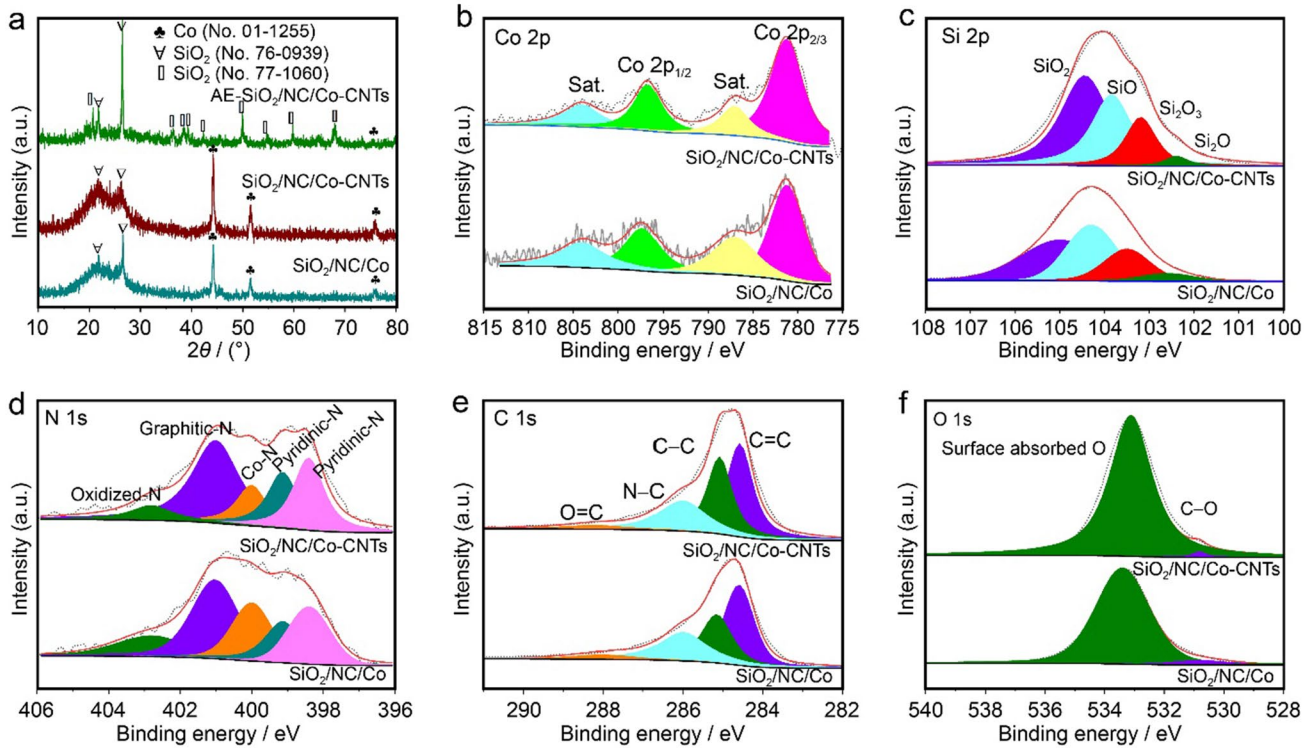

Fig. 2 **a** XRD patterns of the catalysts; XPS spectra of **b** Co 2p, **c** Si 2p, **d** N 1s, **e** C 1s, and **f** O 1s of SiO_2/NC/Co and SiO_2/NC/Co-CNTs catalysts

The morphologies of the as-prepared catalysts were observed by scanning electron microscope (SEM), as shown in Fig. 3. The SiO_2/NC/Co catalyst exhibits that numerous uniform SiO_2 nanospheres with a diameter of ~ 100 nm are tightly anchored on ultrathin carbon nanosheets, forming a stable matrix (Figs. 3a–c, S4). Furthermore, numerous porous structures are observed in the SiO_2/NC/Co catalyst, which is due to the carbon pores caused by the drop of SiO_2 nanospheres. After adding a soft template (basic zinc carbonate), the obtained SiO_2/NC/Co-CNTs catalysts clearly show a prominent hollow carbon tubular structure (Figs. 3d–f, S5). Apparently, the basic zinc carbonate plays a significance part in the formation of tubular structures during heat treatment. Meanwhile, numerous CNTs with a length of ~ 500 nm and a diameter of ~ 60 nm, acting as a conductive channel, are grown from the matrix (Fig. 3f). In addition, the nanoparticles encapsulated at the end of CNTs can be assigned to Co nanoparticles (diameter of ~ 100 nm) (Fig. 3g), which shows high dispersion behavior. Figure S6 further confirms that some Co nanoparticles are encapsulated at the end of CNTs. The element distribution in SiO_2/NC/Co-CNTs catalysts was analyzed by energy-dispersive X-ray spectroscopy (EDS), and it was found that each element (Co, Si, N, O, C) is uniformly distributed on the catalysts (Figs. 3h, S7). N_2 adsorption–desorption spectrum in Fig. 3i indicates the high Brunauer–Emmett–Teller (BET) specific surface area of 112.4 $m^2 \cdot g^{-1}$ for SiO_2/NC/Co-CNTs, which can expose more active sites. The pore distribution in the inset of Fig. 3i demonstrates the abundant mesoporous structure (3.9 nm), which can promote the contact between the electrolyte and the catalyst. On the other hand, after etching SiO_2 nanospheres, it is observed that both the granular and tubular structures disappeared (Fig. S8), which is caused by the facility's collapse during the etching process. For the NC/Co-CNTs catalyst obtained without the addition of SiO_2 nanospheres, there are still a large number of Co nanoparticles encapsulated in CNTs (Fig. S9), while the porous structure disappears, further demonstrating the role of SiO_2 hard templates in constructing 3D porous structures.

TEM is used to further observe the internal microstructure of the SiO_2/NC/Co-CNTs and SiO_2/NC/Co catalysts. For SiO_2/NC/Co catalysts without adding basic zinc carbonate (Fig. 4a–c), the CNTs component is unobservable, further confirming the decisive role of the soft template. Furthermore, the glucose-derived ultra-thin carbon layer is wrapped on the surface of SiO_2 nanospheres, forming an obvious 3D porous heterostructure (Fig. 4b). In addition, the highly dispersed metal Co nanoparticles are firmly fixed in porous carbon matrix assembled by numerous thin carbon nanosheets with thickness of ~ 3 nm (Fig. 4c). After

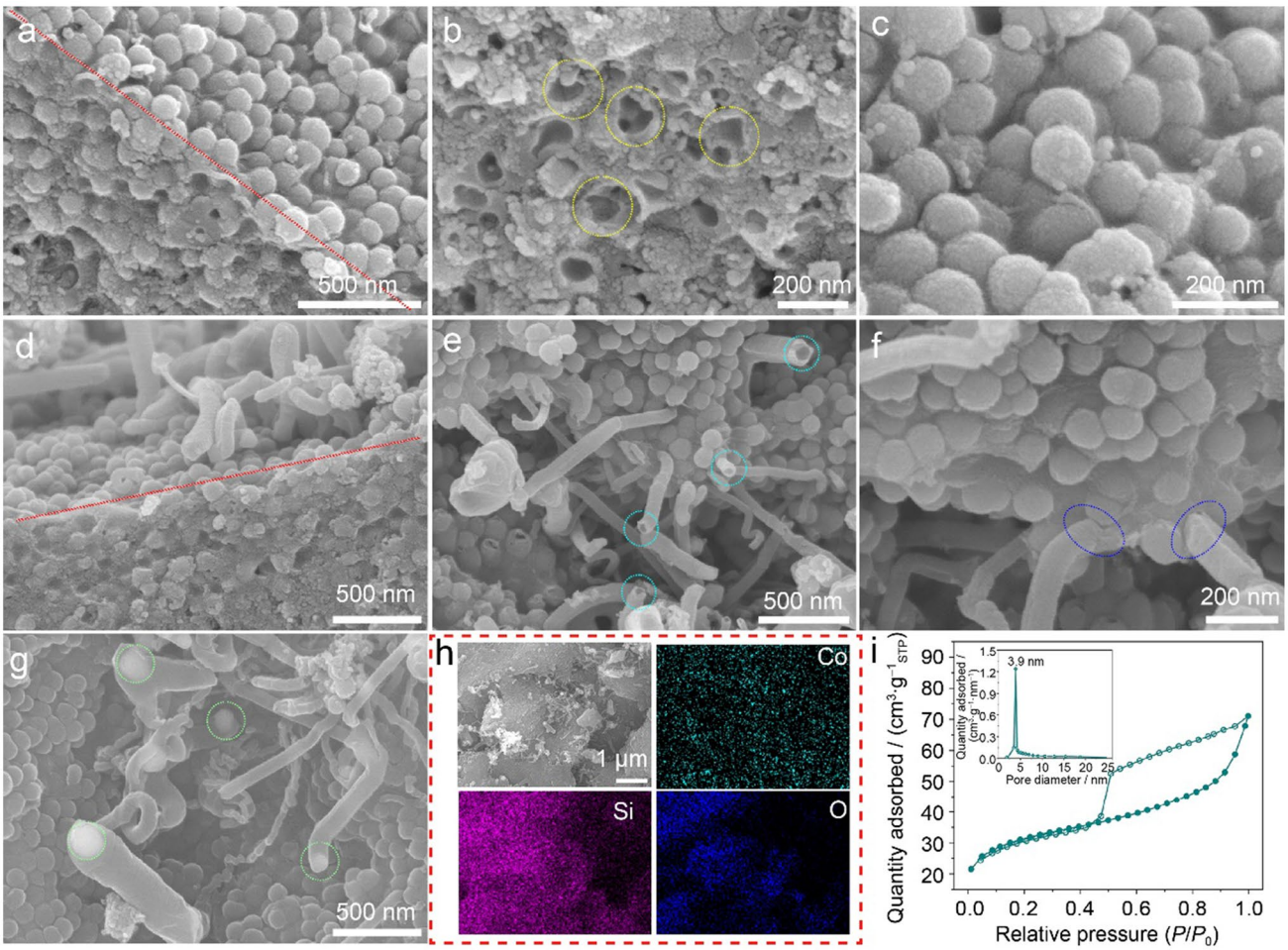

Fig. 3 SEM images of **a**–**c** SiO_2/NC/Co and **d**–**g** SiO_2/NC/Co-CNTs catalysts; **h** EDS elemental mapping of SiO_2/NC/Co-CNTs catalysts; **i** N_2 adsorption–desorption isotherms (insert of pore distribution) of SiO_2/NC/Co-CNTs catalysts

adding basic zinc carbonate, the formed SiO_2/NC/Co-CNTs catalysts contain many highly dispersed Co nanoparticles (Figs. 4d, S10), which are confined to SiO_2 matrix and carbon carriers with high conductivity. Furthermore, bamboo-like CNTs are closely connected with the matrix to form a conductive network. Figure 4e, f shows the high-resolution TEM (HRTEM) images of SiO_2/NC/Co-CNTs. Clearly, Co nanoparticles are coated by thin carbon with several layers, which acts as "armor" to limit the growth of Co nanoparticles and protect the metallic Co from oxidation [48]. The bamboo-like CNTs are highly graphitized with a lattice spacing of 0.34 nm. The hollow structure inside bamboo-like CNTs is conducive to shorten the electron transmission path and enhance the electron transmission capacity. HRTEM image in Fig. 4g detects the (111) plane of metallic Co with a lattice spacing of 0.21 nm [49]. EDS element mapping image indicates that Si and O elements are uniformly distributed throughout SiO_2/NC/Co-CNTs catalyst, Co elements are located on Co nanoparticles, while N and C elements are centered on carbon matrix and CNTs. The above results fully demonstrate the successful preparation of the 3D porous SiO_2/NC/Co-CNTs catalyst under the action of double templates.

It is expected that the SiO_2/NC/Co-CNTs catalysts with excellent stability, abundant nitrogen heteroatoms doping, and highly dispersed metal active sites will provide strong electrocatalytic kinetics. Therefore, the OER performance of the catalysts is investigated. As shown in the LSV polarization curves (Fig. 5a), the as-synthesized SiO_2/NC/Co-CNTs catalyst requires an overpotential of only 298 mV (1.528 vs. RHE) to achieve a current density (j) of 10 mA·cm^{-2}, which is lower than the norm RuO_2 (330 mV, 1.560 V vs. RHE). The robust activity (298 mV@10 mA·cm^{-2}) for the SiO_2/NC/Co-CNTs catalyst is superior to that of many latest OER catalysts, as listed in Table S1. The electrocatalytic active surface area (ECSA)–correct LSV curve of the catalyst in Fig. S11 shows that SiO_2/NC/Co-CNTs exhibits the lowest onset potential and the highest current density at a

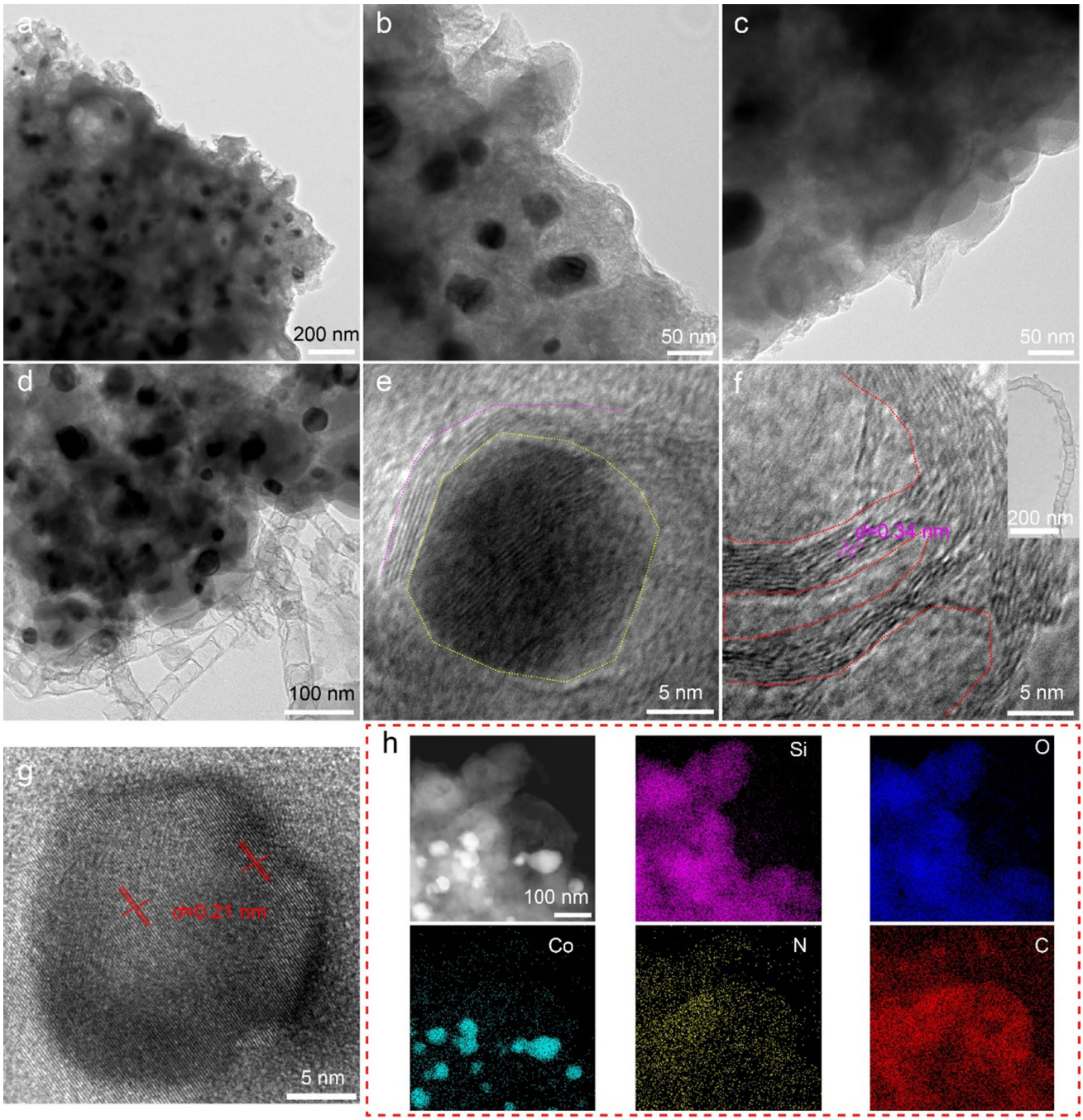

Fig. 4 **a–d** TEM and **e–g** HRTEM images of **a–c** SiO_2/NC/Co and **d–g** SiO_2/NC/Co-CNTs catalysts; **h** EDS mapping image of SiO_2/NC/Co-CNTs catalysts

given potential, indicating its higher intrinsic OER activity. In contrast, the SiO_2/NC/Co catalyst has weak OER activity with an overpotential of 519 mV, indicating the importance of basic zinc carbonate as a soft template in controlling catalyst morphology and improving catalyst activity. The optimized content of basic zinc carbonate in SiO_2/NC/Co-CNTs catalysts for the OER process is 0.3 g (Fig. S12). Likewise, the OER activity of NC/Co-CNTs without adding SiO_2 nanospheres is also poor (444 mV@10 mA·cm^{-2}). NC/Co-CNTs catalysts with different content of SiO_2 nanospheres display relatively different OER activities (Fig. S13). It can be confirmed that SiO_2 as a hard template with appropriate content can improve the activity of the catalyst. Importantly, after AE, the OER activity of AE-SiO_2/NC/Co-CNTs declined (402 mV@10 mA·cm^{-2}), which is due to the collapse of the framework, as confirmed by the above

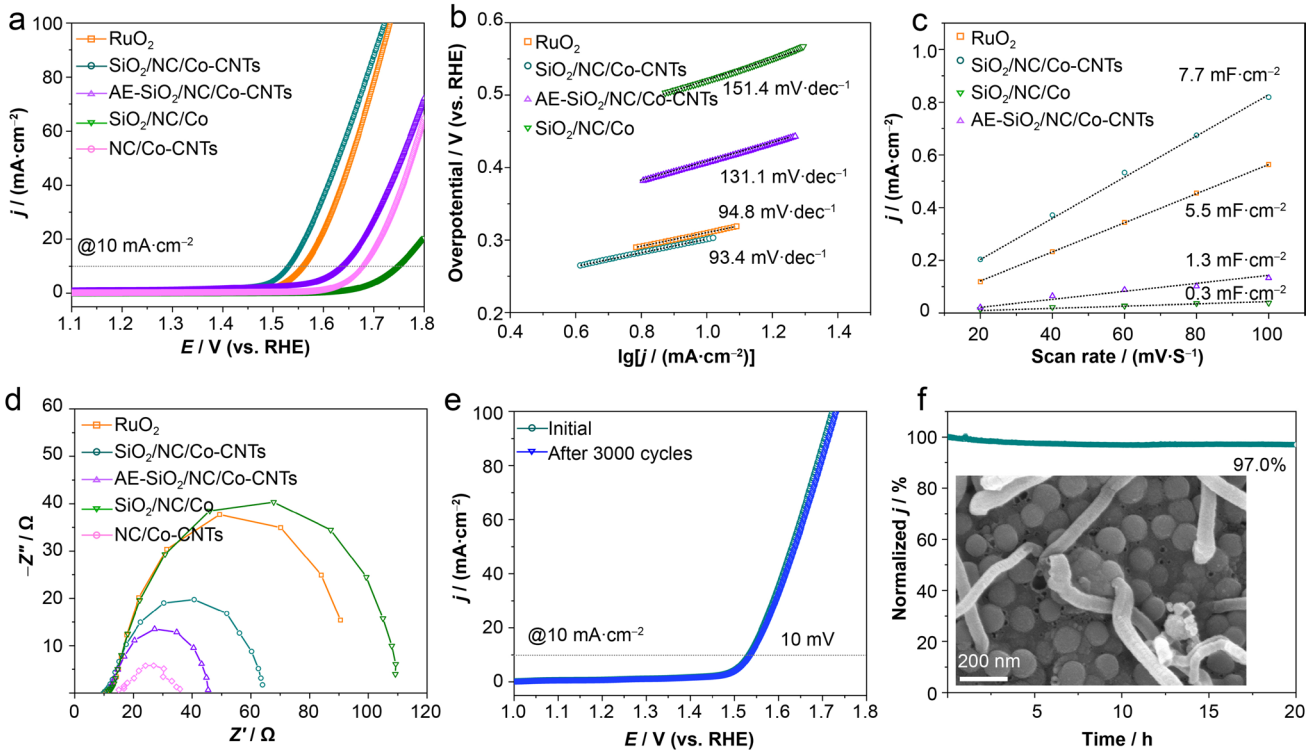

Fig. 5 **a** LSV curves; **b** Tafel slopes; **c** C_{dl} values, and **d** EIS spectra of the catalysts; **e** CV cycling and **f** long-term stability test of SiO_2/NC/Co-CNTs catalyst (Insert: SEM image of SiO_2/NC/Co-CNTs catalyst after long-term stability test)

SEM results. In addition, urea plays an important role as a nitrogen and partial carbon source. Thus, the OER activity of catalysts with different contents of urea is investigated (Fig. S14), indicating that the optimized content of urea is 40 mmol. The electrochemical kinetics of different electrocatalysts were evaluated by Tafel slope. The smaller the Tafel slope, the faster the reaction kinetics, the better the performance of the catalyst. As shown in Fig. 5b, the Tafel slope of SiO_2/NC/Co-CNTs catalyst (93.4 mV·dec^{-1}) is the lowest, which is close to that of standard RuO_2 (94.8 mV·dec^{-1}) and lower than that of AE-SiO_2/NC/Co-CNTs (131.1 mV·dec^{-1}) and SiO_2/NC/Co (151.4 mV·dec^{-1}), revealing better OER electrocatalytic kinetics for SiO_2/NC/Co-CNTs [50].

CV curves recorded at different scan rates to evaluate the electrochemical double-layer capacitance (C_{dl}), which is an important indication for insight into the intrinsic catalytic activity. According to the CV curves, the C_{dl} values of the samples are calculated, as shown in Fig. 5c. Obviously, compared to the C_{dl} values of AE-SiO_2/NC/Co-CNTs (1.3 mF·cm^{-2}), SiO_2/NC/Co (0.3 mF·cm^{-2}), and RuO_2 (5.5 mF·cm^{-2}), SiO_2/NC/Co-CNTs catalyst enables the largest C_{dl} value of 7.7 mF·cm^{-2}, which indicates the strong intrinsic activity for SiO_2/NC/Co-CNTs. Furthermore, the ECSA of the electrocatalyst can be calculated using the equation of ECSA = C_{dl}/C_s, where C_s is the specific capacitance of a flat surface (0.04 mF·cm^{-2}) [51]. As shown in Fig. S15, SiO_2/NC/Co-CNTs exhibit the highest ECSA value of 192.5. The results verify that the SiO_2/NC/Co-CNTs catalyst can provide more exposed active sites and inherit higher intrinsic activity. At the same time, EIS is performed to deeply understand the electron transfer kinetics of the OER process. Figure 5d presents that SiO_2/NC/Co-CNTs catalyst enables the more negligible charge-transfer resistance (R_{ct}, 44.5 Ω), and the best reaction kinetics were confirmed. However, the commercial RuO_2 (66.8 Ω) shows larger R_{ct} values. In addition, the contact resistance (R_s) for SiO_2/NC/Co-CNTs catalyst is about 10 Ω, indicating its small resistance and good ion response. The high conductivity of graphitic carbon matrix and 1D CNTs is believed to contribute to the strong reaction kinetics and good ion response of SiO_2/NC/Co-CNTs.

Long-term stability is an important index to evaluate the performance changes in electrocatalysis applications. Therefore, the LSV curves of SiO_2/NC/Co-CNTs before and after 3000 continuing CV cycles are recorded, as shown in Fig. 5e. Clearly, at a current density of 10 mA·cm^{-2}, the overpotential decays by 10 mV, suggesting the excellent long-term stability for SiO_2/NC/Co-CNTs. On the side, we further evaluated the stability of SiO_2/NC/Co-CNTs catalysts under a continuous OER process at a constant potential of 1.531 V (vs. RHE). As shown in Fig. 5f, the current density remains 97% during the 20 h test period. Notably, there

are no important changes in the morphology and structure of the SiO_2/NC/Co-CNTs catalyst after the long-term stability test (insert of Figs. 5f, S16). The structure of the catalyst retains the integrity of the highly dispersed Co nanoparticles, this can be attributed to the stable catalyst structure induced by the dual-template strategy. In addition, after 100 h of stability test, the current density can still maintain 90.5%, further revealing the good catalytic stability of SiO_2/NC/Co-CNTs catalysts.

4 Conclusions

In summary, a 3D porous SiO_2/NC/Co-CNTs heterostructure with highly dispersed Co nanoparticles, CNTs conductive channels, and abundant nitrogen heteroatoms doping are reasonably constructed by a dual template strategy. The SiO_2 hard template can provide a 3D porous structure, increase the specific surface area, and promote the contact area of the electrolyte. At the same time, the basic zinc carbonate soft template can control the growth of 1D CNTs and facilitate the exposure of the active sites. Therefore, SiO_2/NC/Co-CNTs catalyst inherits excellent OER activity with a low overpotential (298 mV@10 $mA{\cdot}cm^{-2}$). In addition, SiO_2/NC/Co-CNTs catalyst enables good long-term durability with a 10 mV decay in overpotential after 3000 CV cycles, and 97% remain in current density over 20 h. This is beneficial from the stable 3D structure and the close combination of Co/SiO_2 nanoparticles with carbon carriers. This study provides a new strategy for fine construction of hard and soft dual templates with highly dispersed active sites in electrocatalysts.

Supplementary Information The online version contains supplementary material available at https://doi.org/10.1007/s42864-023-00253-x.

Acknowledgements This work was supported by the National Natural Science Foundation of China (No. 22269010), Jiangxi Provincial Natural Science Foundation (No. 20224BAB214021), the Training Program for Academic and Technical Leaders of Major Disciplines in Jiangxi Province (No. 20212BCJ23020), and the Science and Technology Project of Jiangxi Provincial Department of Education (No. GJJ211305).

Data availability The data generated during and/or analyzed in this article are available from the corresponding author on reasonable request.

Declarations

Conflict of interest The authors declare no conflict of interest.

References

1. Wu JS, Yang T, Fu R, Zhou M, Xia LX, Wang ZY, Zhao Y. Constructing electrocatalysts with composition gradient distribution by solubility product theory: amorphous/crystalline CoNiFe-LDH hollow nanocages. Adv Funct Mater. 2023;33(37):2300808. https://doi.org/10.1002/adfm.202300808.
2. Zhao X, He DP, Xia BY, Sun YJ, You B. Ambient electrosynthesis toward single-atom sites for electrocatalytic green hydrogen cycling. Adv Mater. 2023;35(14):2210703. https://doi.org/10.1002/adma.202210703.
3. Wang JH, Yang SW, Ma FB, Zhao YK, Zhao SN, Xiong ZY, Cai D, Shen HD, Zhu K, Zhang QY, Cao YL, Wang TS, Zhang HP. RuCo alloy nanoparticles embedded within N-doped porous two-dimensional carbon nanosheets: a high-performance hydrogen evolution reaction catalyst. Tungsten. 2023. https://doi.org/10.1007/s42864-023-00223-3.
4. Yan WJ, Zhang JT, Lv AJ, Lu SL, Zhong YW, Wang MY. Self-supporting and hierarchically porous NixFe–S/NiFe2O4 heterostructure as a bifunctional electrocatalyst for fluctuating overall water splitting. Int J Miner Metall Mater. 2022;29(5):1120. https://doi.org/10.1007/s12613-022-2443-2.
5. Han F, Xu W, Jia CX, Chen XT, Xie YP, Zhen C, Liu G. Triggering heteroatomic interdiffusion in one-pot-oxidation synthesized NiO/$CuFeO_2$ heterojunction photocathodes for efficient solar hydrogen production from water splitting. Rare Met. 2023;42:853. https://doi.org/10.1007/s12598-022-02177-w.
6. Zhang SC, Tan CH, Yan RP, Zou XF, Hu FL, Mi Y, Yan C, Zhao SL. Constructing built-in electric field in heterogeneous nanowire arrays for efficient overall water electrolysis. Angew Chem Int Ed. 2023;135(26): e202302795. https://doi.org/10.1002/anie.202302795.
7. Ma MY, Yu HZ, Deng LM, Wang LQ, Liu SY, Pan H, Ren JW, Maximov Y, Hu F, Peng SJ. Interfacial engineering of heterostructured carbon-supported molybdenum cobalt sulfides for efficient overall water splitting. Tungsten. 2023;5:589. https://doi.org/10.1007/s42864-023-00212-6.
8. Zeng XJ, Ye YF, Wang YQ, Yu RH, Moskovits M, Stucky GD. Honeycomb-like MXene/$NiFeP_x$-NC with "continuous" single-crystal enabling high activity and robust durability in electrocatalytic oxygen evolution reactions. J Adv Ceram. 2023;12(3):553. https://doi.org/10.26599/JAC.2023.9220704.
9. Dong MY, Fu HQ, Xu YM, Zou Y, Chen ZY, Wang L, Hu MQ, Zhang KD, Fu B, Yin HJ, Liu PR, Zhao HJ. NiCo alloy-anchored self-supporting carbon foam as a bifunctional oxygen electrode for rechargeable and flexible Zn-air batteries. Battery Energy. 2023;2(4):20220063. https://doi.org/10.1002/bte2.20220063.
10. Zeng XJ, Zhang HQ, Yu RH. Trace tiny NiCo alloy nanoparticles encapsulated on hierarchical porous peanut-like carbon walls for robust oxygen evolution reaction. J Alloy Comp. 2023;960:170950. https://doi.org/10.1016/j.jallcom.2023.170950.
11. Zeng XJ, Choi SM, Bai YC, Jang MJ, Yu RH, Cho HS, Kim CH, Myung NV, Yin YD. Plasmon-enhanced oxygen evolution catalyzed by Fe_2N-embedded TiO_xN_y nanoshells. ACS Appl Energy Mater. 2020;3(1):146. https://doi.org/10.1021/acsaem.9b02022.
12. Yoon H, Ju B, Kim DW. Perspectives on the development of highly active, stable, and cost-effective OER electrocatalysts in acid. Battery Energy. 2023;2(5):20230017. https://doi.org/10.1002/bte2.20230017.
13. Sun YQ, Li XL, Zhang T, Xu K, Yang YS, Chen GZ, Li CC, Xie Y. Nitrogen-doped cobalt diselenide with cubic phase maintained for enhanced lkaline hydrogen evolution. Angew Chem. 2021;133(39):21745. https://doi.org/10.1002/anie.202109116.
14. Fan WJ, Duan ZY, Liu W, Mehmood R, Qu JT, Cao YC, Guo XY, Zhong J, Zhang FX. Rational design of heterogenized molecular phthalocyanine hybrid single-atom electrocatalyst towards two-electron oxygen reduction. Nat Commun. 2023;14(1):1426. https://doi.org/10.1038/s41467-023-37066-y.
15. Pan Y, Lin R, Chen YJ, Liu SJ, Zhu W, Cao X, Chen WX, Wu KL, Cheong WC, Wang Y, Zheng LR, Luo J, Lin Y, Liu YQ, Liu CG, Li J, Lu Q, Chen X, Wang DS, Peng Q, Chen C, Li YD. Design

of single-atom Co-N_5 catalytic site: a robust electrocatalyst for CO_2 reduction with nearly 100% CO selectivity and remarkable stability. J Am Chem Soc. 2018;140(12):4218. https://doi.org/10.1021/jacs.8b00814.
16. Zhu YQ, Sun WM, Luo J, Chen WX, Cao T, Zheng LR, Dong JC, Zhang J, Zhang ML, Han YH, Chen C, Peng Q, Wang DS, Li YD. A cocoon silk chemistry strategy to ultrathin N-doped carbon nanosheet with metal single-site catalysts. Nat Commun. 2018;9(1):3861. https://doi.org/10.1038/s41467-018-06296-w.
17. Nguyen TV, Tekalgne M, Nguyen TP, Le QV, Ahn SH, Kim SY. Electrocatalysts based on MoS_2 and WS_2 for hydrogen evolution reaction: an overview. Battery Energy. 2023;2(3):20220057. https://doi.org/10.1002/bte2.20220057.
18. Wang YX, Cui XZ, Zhang JQ, Qiao JL, Huang HT, Shi JL, Wang GX. Advances of atomically dispersed catalysts from single-atom to clusters in energy storage and conversion applications. Prog Mater Sci. 2022;128:100964. https://doi.org/10.1016/j.pmatsci.2022.100964.
19. Dong F, Wu MJ, Chen ZS, Liu XH, Zhang GX, Qiao JL, Sun SL. Atomically dispersed transition metal-nitrogen-carbon bifunctional oxygen electrocatalysts for zinc-air batteries: Recent advances and future perspectives. Nano-Micro Lett. 2022;14(1):36. https://doi.org/10.1007/s40820-021-00768-3.
20. Wu M, Zhang G, Chen N, Hu Y, Regier T, Rawach D, Sun S. Self-reconstruction of Co/Co_2P heterojunctions confined in N-doped carbon nanotubes for zinc-air flow batteries. ACS Energy Lett. 2021;6(4):1153. https://doi.org/10.1021/acsenergylett.1c00037.
21. Zhang JJ, Liu W, He F, Song M, Huang X, Shen T, Li JW, Zhang C, Zhang J, Wang DL. Highly dispersed Co atoms anchored in porous nitrogen-doped carbon for acidic H_2O_2 electrosynthesis. Chem Eng J. 2022;438: 135619. https://doi.org/10.1016/j.cej.2022.135619.
22. Yu H, Zeng YX, Li NW, Luan DY, Yu L, Lou XW. Confining Sn nanoparticles in interconnected N-doped hollow carbon spheres as hierarchical zincophilic fibers for dendrite-free Zn metal anodes. Sci Adv. 2022;8(10):eabm5766. https://doi.org/10.1126/sciadv.abm5766.
23. Liu XH, Zhai XW, Sheng WB, Tu J, Zhao ZY, Shi YL, Xu CX, Ge GX, Jia X. Isolated single iron atoms anchored on a N, S-codoped hierarchically ordered porous carbon framework for highly efficient oxygen reduction. J Mater Chem A. 2021;9(16):10110. https://doi.org/10.1039/D1TA00384D.
24. Zhong L, Zhou H, Li RF, Cheng H, Wang S, Chen BY, Zhuang YY, Chen JF, Yuan AH. Co/CoO_x heterojunctions encapsulated N-doped carbon sheets via a dual-template-guided strategy as efficient electrocatalysts for rechargeable Zn-air battery. J Colloid Interf Sci. 2021;599:46. https://doi.org/10.1016/j.jcis.2021.04.084.
25. Liu F, Zhang XQ, Zhang XL, Wang LL, Liu MM, Zhang JJ. Dual-template strategy for electrocatalyst of cobalt nanoparticles encapsulated in nitrogen-doped carbon nanotubes for oxygen reduction reaction. J Colloid Interf Sci. 2021;581:523. https://doi.org/10.1016/j.jcis.2020.07.008.
26. Li W, Zhao DY. Extension of the stober method to construct mesoporous SiO_2 and TiO_2 shells for uniform multifunctional core-shell structures. Adv Mater. 2013;25(1):142. https://doi.org/10.1002/adma.201203547.
27. Buchel G, Unger KK, Matsumoto A, Tsutsumi K. A novel pathway for synthesis of submicrometer-size solid core/mesoporous shell silica spheres. Adv Mater. 1988;10(13):1036. https://doi.org/10.1002/(SICI)1521-4095(199809)10:13%3c1036::AID-ADMA1036%3e3.0.CO;2-Z.
28. Shu XX, Chen QW, Yang MM, Liu MM, Ma JZ, Zhang JT. Tuning Co-catalytic sites in hierarchical porous N-doped carbon for high-performance rechargeable and flexible Zn-air battery. Adv Energy Mater. 2023;13(1):2202871. https://doi.org/10.1002/aenm.202202871.
29. Kisand K, Sarapuu A, Kikas A, Kisand V, Rähn M, Treshchalov A, Käärik M, Piirsoo HM, Aruväli J, Paiste P, Leis J, Sammelselg V, Tamm A, Tammeveski K. Bifunctional multi-metallic nitrogen-doped nanocarbon catalysts derived from 5-methylresorcinol. Electrochem Commun. 2021;124: 106932. https://doi.org/10.1016/j.elecom.2021.106932.
30. Xu XQ, Xie JH, Liu B, Wang RY, Liu MY, Zhang J, Liu J, Cai Z, Zou JL. PBA-derived FeCo alloy with core-shell structure embedded in 2D N-doped ultrathin carbon sheets as a bifunctional catalyst for rechargeable Zn-air batteries. Appl Catal B-Environ. 2022;316: 121687.
31. Ban JJ, Xu HJ, Cao GQ, Fan YM, Pang WK, Shao GS, Hu JH. Synergistic effects of phase transition and electron-spin regulation on the electrocatalysis performance of ternary nitride. Adv Funct Mater. 2023;33(25):2300623. https://doi.org/10.1002/adfm.202300623.
32. Li XG, Zhou JH, Liu C, Xu L, Lu CL, Yang J, Pang H, Hou WH. Encapsulation of janus-structured Ni/Ni_2P nanoparticles within hierarchical wrinkled N-doped carbon nanofibers: Interface engineering induces high-efficiency water oxidation. Appl Catal B-Environ. 2021;298: 120578. https://doi.org/10.1016/j.apcatb.2021.120578.
33. Liu YF, Ren TL, Su ZJ, Li CJ. Nanoflower-like MoS_2 anchored on electrospun carbon nanofibers-interpenetrated reduced graphene oxide as microbial fuel cells anode achieving high power density. J Mater Chem A. 2023;11(19):10371. https://doi.org/10.1039/D3TA01265D.
34. Fan XM, Cai T, Wang SY, Yang ZH, Zhang WX. Carbon nanotube-reinforced dual carbon stress-buffering for highly stable silicon anode material in lithium-ion battery. Small. 2023;19(30):2300431. https://doi.org/10.1002/smll.202300431.
35. Liu HY, Joo JB, Dahl M, Fu LS, Zeng ZZ, Yin YD. Crystallinity control of TiO_2 hollow shells through resin-protected calcination for enhanced photocatalytic activity. Energy Environ Sci. 2015;8(1):286. https://doi.org/10.1039/C4EE02618G.
36. Lee DH, Lee BH, Sinha AK, Park JH, Kim MS, Park JJ, Shin HJ, Lee KS, Sung YE, Hyeon T. Engineering titanium dioxide nanostructures for enhanced lithium-ion storage. J Am Chem Soc. 2018;140(48):16676. https://doi.org/10.1021/jacs.8b09487.
37. Zeng XJ, Zhang QQ, Jin CL, Huang H, Gao YF. Fe-induced electronic transfer and structural evolution of lotus pod-like CoNiFeP_x@P, N-C heterostructure for sustainable oxygen evolution. Energy Environ Mater. 2023;2023:e12628. https://doi.org/10.1002/eem2.12628.
38. Qin MC, Fan SY, Li XY, Yin ZF, Wang L, Chen A. Double active sites in Co-N_x-C@Co electrocatalysts for simultaneous production of hydrogen and carbon monoxide. ACS Appl Mater Interfaces. 2021;13(32):38256. https://doi.org/10.1021/acsami.1c08363.
39. Zeng XJ, Zhang HQ, Zhang XF, Zhang QQ, Chen YX, Yu RH, Moskovits M. Coupling of ultrasmall and small Co_xP nanoparticles confined in porous SiO_2 matrix for a robust oxygen evolution reaction. Nano Mater Sci. 2022;4(4):393. https://doi.org/10.1016/j.nanoms.2022.03.002.
40. Cao ZQ, Wu MQ, Hu HB, Liang GJ, Zhi CY. Monodisperse Co_9S_8 nanoparticles *in situ* embedded within N, S-codoped honeycomb-structured porous carbon for bifunctional oxygen electrocatalyst in a rechargeable Zn-air battery. NPG Asia Mater. 2018;10(7):670. https://doi.org/10.1038/s41427-018-0063-0.
41. Zhou PY, Wang LM, Lv JJ, Li RS, Gao FY, Huang XB, Lu YF, Wang G. Tuning the electronic structure of Co@N-C hybrids via metal-doping for efficient electrocatalytic hydrogen evolution reaction. J Mater Chem A. 2022;10(9):4981. https://doi.org/10.1039/D1TA08226D.

42. Zeng XJ, Zhao C, Yin YC, Nie TL, Xie NH, Yu R, Stucky GD. Construction of $NiCo_2O_4$ nanosheets-covered $Ti_3C_2T_x$ MXene heterostructure for remarkable electromagnetic microwave absorption. Carbon. 2022;193:26. https://doi.org/10.1016/j.carbon.2022.03.029.
43. Zeng XJ, Zhao C, Jiang X, Yu RH, Che RC. Functional tailoring of multi-dimensional pure MXene nanostructures for significantly accelerated electromagnetic wave absorption. Small. 2023;19(41):2303393. https://doi.org/10.1002/smll.202303393.
44. Men YN, Li P, Zhou JH, Cheng GZ, Chen SL, Luo W. Tailoring the electronic structure of Co_2P by N doping for boosting hydrogen evolution reaction at all pH values. ACS Catal. 2019;9(4):3744. https://doi.org/10.1021/ACSCATAL.9B00407.
45. Zeng XJ, Wu ZM, Nie TL, Zhao C, Yu RH, Stucky GD, Gao YF. Metal/N-doped carbon nanoparticles derived from metal-organic frameworks for electromagnetic wave absorption. ACS Appl Nano Mater. 2022;5(8):11474. https://doi.org/10.1021/acsanm.2c02513.
46. Zhang XY, Wei L, Guo X. Ultrathin mesoporous $NiMoO_4$-modified MoO_3 core/shell nanostructures: enhanced capacitive storage and cycling performance for supercapacitors. Chem Eng J. 2018;353:615. https://doi.org/10.1016/j.cej.2018.07.160.
47. Wang D, Chang YX, Li YR, Zhang SL, Xu SL. Well-dispersed $NiCoS_2$ nanoparticles/rGO composite with a large specific surface area as an oxygen evolution reaction electrocatalyst. Rare Met. 2021;40:3156. https://doi.org/10.1007/s12598-021-01733-0.
48. Hu YZ, Guo XY, Shen T, Zhu Y, Wang DL. Hollow porous carbon-confined atomically ordered $PtCo_3$ intermetallics for an efficient oxygen reduction reaction. ACS Catal. 2022;12(9):5380. https://doi.org/10.1021/acscatal.2c01541.
49. Zeng XJ, Tan YN, Xia L, Zhang QQ, Stucky GD. MXene-derived Ti_3C_2-Co-TiO_2 nanoparticle arrays via cation exchange for highly efficient and stable electrocatalytic oxygen evolution. Chem Commun. 2023;59(7):880. https://doi.org/10.1039/D2CC05911H.
50. Zeng XJ, Zhang HQ, Yu RH, Stucky GD, Qiu JS. A phase and interface co-engineered MoP_xS_y@$NiFeP_xS_y$@NPS-C hierarchical heterostructure for sustainable oxygen evolution reaction. J Mater Chem A. 2023;11(26):14272. https://doi.org/10.1039/D3TA01993D.
51. Zeng XJ, Duan DR, Zhang XY, Li XH, Li K, Yu RH, Moskovits M. Doping and interface engineering in a sandwich $Ti_3C_2T_x$/$MoS_{2-x}P_x$ heterostructure for efficient hydrogen evolution. J Mater Chem C. 2022;10(11):4140. https://doi.org/10.1039/D1TC05974B.